Improved spectral estimation of equatorial spread F through aperiodic pulsing and Bayesian inversion

D. L. Hysell,[1] J. L. Chau,[2] and S. Lakshmanan[3]

[1] Observations of coherent scatter from plasma density irregularities associated with equatorial spread F made at Jicamarca with aperiodic radar pulses are presented. Aperiodic pulses are used to resolve range and frequency aliasing of the moderately overspread target. Two strategies are considered in which the radar interpulse period undergoes small and large variations, respectively. Both strategies perform satisfactorily, although the latter provides autocorrelation functions sampled more uniformly in time, which is advantageous, particularly when few samples are available. The nonuniformly sampled radar data that result are analyzed using a Bayesian approach based on maximum entropy. A scenario for combining aperiodic pulsing and spaced-receiver radar imaging for observing spread F is described. With this technique, it may be possible to estimate the irregularity power and energy spectral density versus wave number.

1. Introduction

[2] This is a report on continuing efforts at Jicamarca to measure the Doppler spectra of moderately overspread targets in the ionosphere using aperiodically spaced radar pulses. The targets in question are field-aligned plasma density irregularities observed after sunset during periods of strong equatorial spread F (ESF). It is not uncommon for ionospheric irregularities to extend over 1500 km in altitude at Jicamarca, particularly at solar maximum. The radar pulse repetition frequency must therefore be less than 100 Hz in order to avoid range aliasing. However, the corresponding band of Doppler velocities that can be measured without frequency aliasing at 50 MHz, ±150 m/s, is narrower than the actual range exhibited by the echoes by up to a factor of about 10 [*Hysell et al.*, 1994]. The target is therefore overspread at 50 MHz. Most often, the factor is more like 2–4, so the target is only moderately overspread.

Even so, unambiguous spectral estimation has historically been unreliable at best.

[3] We are interested in measuring the Doppler spectra of ESF on general grounds but also with a specific application in mind. Using a formalism developed by *Montgomery* [1975] to describe turbulent diffusion in guiding center plasmas, *Hysell and Chau* [2004] proposed a theory for the shape of the coherent scatter spectra associated with plasma turbulence in ESF. The theoretical shape was hybrid Gaussian-Lorentzian with a width that depends on the turbulent energy within the scattering volume. The theory is only applicable to strongly driven flows in the topside F region thought to occur when the ionospheric interchange instability underlying ESF enters its inertial regime [*Zargham and Seyler*, 1989]. The occurrence of inertial range turbulence in ESF is thought to be predictable [*McDaniel and Hysell*, 1997; *Shume and Hysell*, 2004], and direct numerical simulation suggests that the spectral model is accurate [*Hysell and Shume*, 2002]. However, experimental validation of the model is lagging, mainly because of the overspread target problem. If the Doppler spectra of the irregularities could be measured, it might be possible through model inversion to infer the wave number distribution of the ionospheric irregularities, something that presently can only be done using spacecraft. Such information is crucial for understanding radio scintillations caused by ESF.

[1] Department of Earth and Atmospheric Sciences, Cornell University, Ithaca, New York, USA.
[2] Radio Observatorio de Jicamarca, Instituto Geofísico del Perú, Lima, Peru.
[3] Raytheon Company, Woburn, Massachusetts, USA.

[4] Range and frequency aliasing are both consequences of periodic radar pulses. Periodic pulsing has the advantage of allowing simple and efficient data analysis through periodograms, discrete Fourier transforms, and (usually) fast Fourier transforms (FFTs). It has the disadvantages of range and frequency ambiguity since there is no way to distinguish aliased and unaliased signals. Variations on the basic radar technique involving double pulses [*Farley*, 1972; *Sahr et al.*, 1989], multiple pulses [*Farley*, 1972], and coded pulses [*Sulzer*, 1986; *Lehtinen and Häggström*, 1987] have been introduced to interrogate overspread targets. A generalization of the multipulse experiment is one which uses long sequences of pulses with aperiodic spacings. This technique is familiar outside aeronomy (e.g., for blind speed mitigation in staggered pulse repetition frequency moving target indicator radar systems [*Levanon*, 1988]) but was introduced to this field only recently by *Uppala* [1993] and *Uppala and Sahr* [1994] and was implemented first at Jicamarca by *Chau et al.* [2004].

[5] Perhaps the most challenging part of aperiodic pulse experiments is the computation of Doppler spectra from the unevenly sampled data that result. One strategy is a complex generalization of the Lomb-Scargle periodogram [*Lomb*, 1976; *Scargle*, 1982], which can be viewed as a linear least squares fit of sine and cosine basis functions to the available data [*Press et al.*, 1988]. In our experience, this technique suffers from poor conditioning and tends to be unstable. The same can be said of interpolative strategies such as Lagrange interpolation. A Kalman filter–based Bayesian strategy was described by *Qi et al.* [2002], and its complex generalization was implemented for aperiodic radar pulse spectral estimation by *Lakshmanan* [2006]. While the technique functioned satisfactorily, it was found to be computationally expensive. Generalized statistical inverse methodology based on singular value decomposition (or its equivalent) incorporating regularization would seem to be an expedient alternative, although we have not attempted it here (see instead *Wingham* [1992]). *Uppala* [1993] experimented with different analysis methods and achieved surprisingly good results by simply neglecting the uneven sampling and proceeding with a periodogram.

[6] In this paper, we treat the analysis of unevenly sampled radar data using Bayesian inversion based on maximum entropy. The method is computationally expedient and can be performed in real time given the pulsing scheme we used. It is essentially the same one used for aperture synthesis imaging at Jicamarca [*Hysell and Chau*, 2006]. Because of this, it should be straightforward to merge the aperiodic pulsing technique with the standard imaging techniques in order to generate spectrally unambiguous radar images of marginally overspread targets like ESF.

2. Radar Experiments

[7] ESF events were observed at Jicamarca using aperiodic radar pulses on 2 September 2002 and again on 21 February 2006. The first of these events, which features well-developed ESF plumes, was already described by *Chau et al.* [2004] and was conducted according to the strategy outlined by *Uppala and Sahr* [1994]. The interpulse period (IPP) T was cycled through 17 similar but distinct values according to the rule $T_i = (67 + i) \times 30 \ \mu s$, $i = 0 \cdots 16$. The average IPP was 2.25 ms or 337.5 km and was short enough to avoid frequency aliasing altogether, which is the key to the strategy. The small jitter in the IPP, meanwhile, was sufficient to resolve ambiguity associated with range aliasing, although range clutter remained (see below).

[8] Receiver samples were acquired at 30 μs (4.5 km) intervals throughout the transmission of the 17 pulses, which continued without interruption. (The receiver was blanked during pulse transmission, causing the loss of a small fraction of the samples.) Because of the short average IPP, each sample contained echoes not only from the most recently transmitted pulse but also from a few of the previous pulses. In processing the data, we regard any sample taken at a time $t = 2r/c$ after any pulse as containing echoes from the range bin r. After 17 pulses were transmitted, there were 17 such samples for every range gate of interest, each with an associated, known sample time.

[9] In general, those samples also contained echoes from many other ranges, representing clutter. Because of the staggered IPP, however, clutter from any given range other than the range of interest appeared at most once per cycle. The clutter was therefore guaranteed to be noise-like (spectrally flat) since echoes from different ranges are expected to be statistically uncorrelated. So long as the signal itself occupies a finite spectral bandwidth, it is possible to estimate and remove the clutter after coherent and incoherent processing. Clutter and actual noise can be distinguished so long as there are a few ranges which are free of the former.

[10] Figure 1 shows a range time intensity (RTI) map for the 2002 event. Note that, for illustrative purposes, we have made no attempt to remove the range clutter bias. For an example of how well clutter removal at this level can work, see *Chau et al.* [2004]. Figure 1 shows some ground clutter near 0 km altitude, equatorial electrojet echoes near 100 km altitude, and ESF echoes spanning altitudes between about 250 and 700 km. Each of these is also a source of range clutter. Range clutter from the ground and the electrojet passes right through
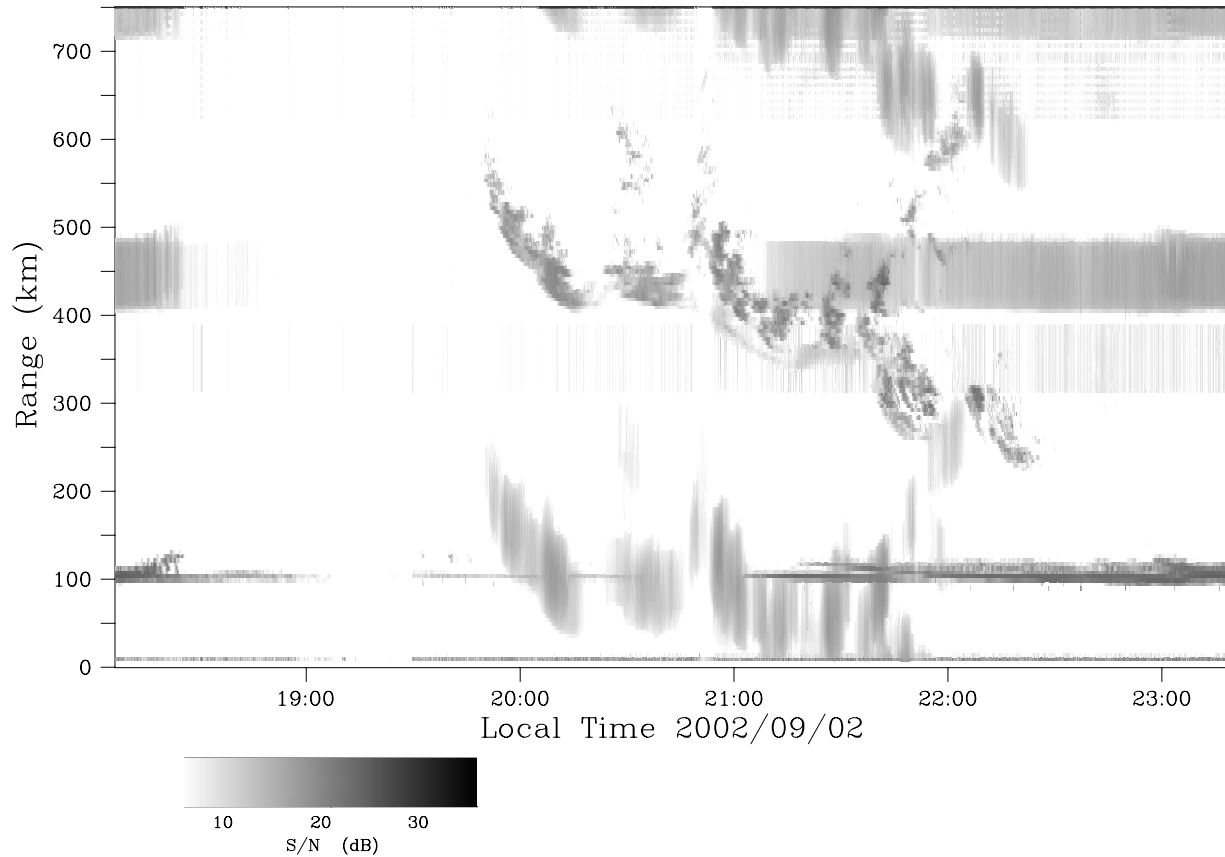
Figure 1. Range time intensity (RTI) plot for an ESF event observed on 2 September 2002 at Jicamarca. No attempt has been made to suppress clutter here.

the spread F echoes, for example. Note how the range clutter "fans out" across contiguous range gates. This is a feature of the "small jitter" strategy.

[11] In some ranges and times, the signal-to-clutter ratio can become quite low. Although the clutter contribution can be removed from the power and spectral estimators, its effect on the statistical confidence of those estimators cannot, so the clutter remains potentially detrimental. The experimental variance of the power estimator in both the time and frequency domains is proportional to $(S + N + C)/S$, where S, N, and C are the true signal, noise, and clutter power, respectively [*Farley*, 1969]. Clutter effects are only truly detrimental if $C \gg S + N$. The efficacy of the aperiodic pulse experiment therefore depends somewhat on where the clutter falls with respect to the signal as well as on the amount of incoherent integration permissible. In this particular example, we are primarily interested in the high-altitude echoes at about 680 km and 2050 LT, where the ratio is not much greater than unity and the likelihood of inertial range flow is also greatest [*Shume and Hysell*, 2004].

[12] A variation on the aperiodic pulse experiment was attempted in 2006. Whereas the 2002 experiment featured an IPP with a small jitter and an average value small enough to satisfy the Nyquist sampling criterion, the 2006 experiment used an IPP with large excursions and included just some intervals small enough to satisfy the criterion. The 17 intervals were chosen pseudorandomly, with a mean value of 2.67 ms (400 km) and extremes of 1.23 ms (184.5 km) and 5.28 ms (792 km). The condition that no clutter from the same range should fall more than once into any other range bin was also maintained. Compared with the original pulsing scheme, this one provides a more uniform distribution of temporal lags for spectral analysis and also distributes clutter more widely in range from its source. These potential improvements come at the expense of a reduced duty cycle, implying the need for longer incoherent integration times to preserve a given degree of statistical confidence. The trade-off is generally favorable since the target in question is usually stationary.

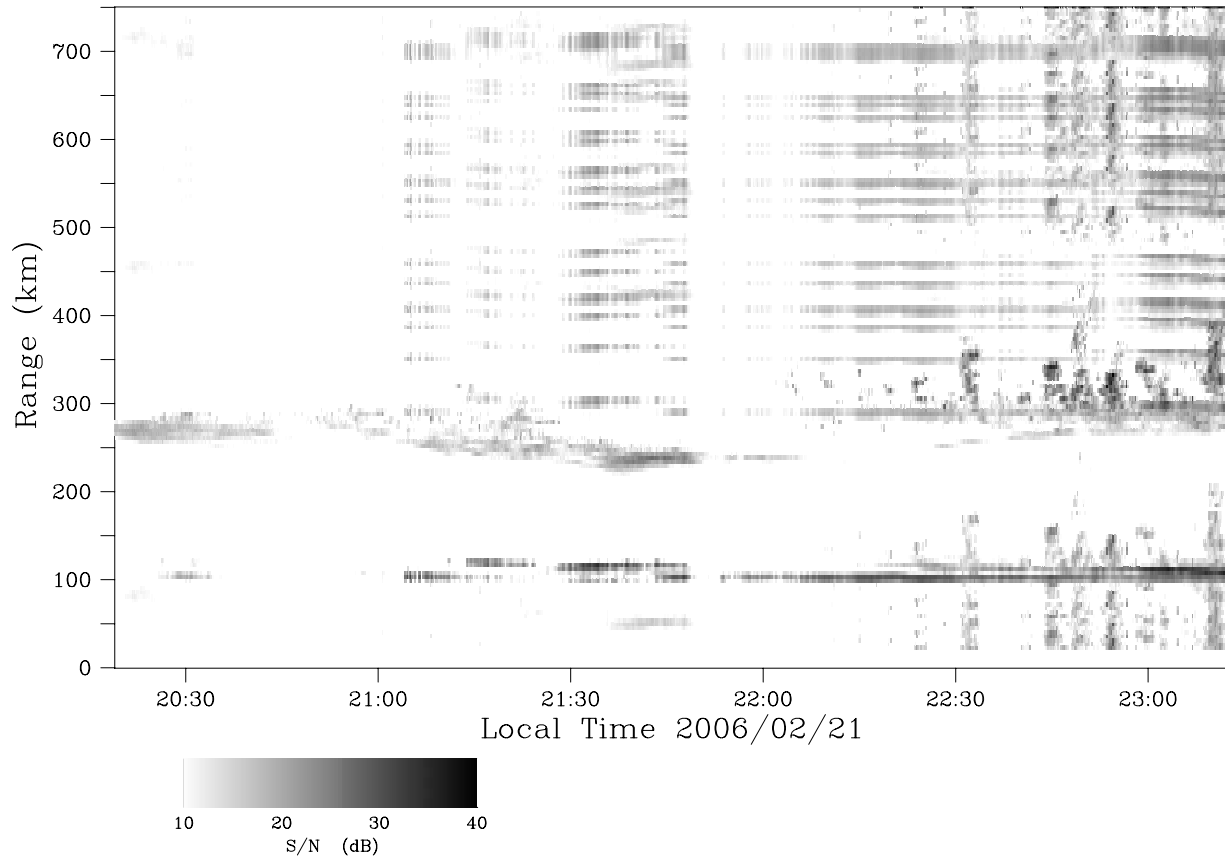[13] Results of the 2006 experiment are shown in Figure 2. Unfortunately, nature produced a weakly

Figure 2.   RTI plot for an ESF event observed on 21 February 2006 at Jicamarca. No attempt has been made to suppress clutter here.

developed spread F event without any topside plumes that was characterized only by a series of small, bottomside plumelets. Although physically uninteresting, this event nevertheless provides the data needed to evaluate the aperiodic pulsing scheme. As before, range clutter from the equatorial electrojet is dispersed throughout the spread F echoes. However, the large gaps provide clutter-free regions for spectral analysis to take place. In any event, the $(S + N + C)/S$ ratio remains close to unity throughout most of the ESF region, so the range clutter is not very detrimental. Once again, it is possible to remove the clutter bias from the RTI image, although the effects on the power estimator variance will remain.

3.   Spectral Analysis

[14]   From a 17 pulse sequence transmitted repeatedly, autocorrelation functions (ACFs) with $(17 \times 16)/2$ distinct lags plus the zero lag can be computed for each radar range of interest. Range clutter vanishes upon correlation in all lags except the zero lag. Statistical

confidence can be improved through incoherent integration as usual. In the case of aperiodic sampling, the lag increments are nonuniform, and we cannot rigorously convert the ACF to Doppler spectra with a discrete Fourier transform.

[15]   The inverse method used here is a Bayesian method which incorporates the Shannon entropy of the target spectrum as a prior probability. The strategy is to find that spectrum which is consistent with the measured ACF within the specified error covariance which has the lowest overall entropy [see, e.g., *Jaynes*, 1982; *Skilling and Bryan*, 1984]. An important feature of this approach is that it admits only positive definite spectra as candidate solutions to the inverse problem. From all the possible spectra consistent with the data, the solution is one that is positive and, in some sense, the smoothest. The maximum entropy algorithm (sometimes called MaxEnt) is in that way an expression of Occam's razor or law of succinctness and provides a resolution of the conditioning problem.

[16]   The particular algorithm is the same one used at Jicamarca for aperture synthesis radar imaging. It was

described recently by *Hysell and Chau* [2006], who also examined error analysis in detail. In the case of radar imaging, the transformation is from visibility to brightness space. Here it is from autocorrelation functions to Doppler spectra. This is a linear transformation and can be written as

$$\mathbf{d} = G\mathbf{m}, \qquad (1)$$

where the data $\mathbf{d}$ is a column vector of autocorrelation function measurements, the model $\mathbf{m}$ is the column vector of sought-after spectral components, and the transformation G is the discrete Fourier transform. We seek the vector $\mathbf{m}$ that satisfies constraint (1) while maximizing the Shannon entropy:

$$S = -\sum \mathbf{m}_i \log(\mathbf{m}_i/M), \qquad (2)$$

where the sum is over all model values and $M \equiv \sum \mathbf{m}_i$ is the total power in the spectrum or, equivalently, the zero lag of the autocorrelation function. This implies extremizing the functional

$$f_1 = S + \lambda^t(\mathbf{d} - G\mathbf{m}) + L(M - \hat{\mathbf{I}}^t\mathbf{m}), \qquad (3)$$

where λ (a column vector) and L are Lagrange multipliers used to enforce the constraints on the model and $\hat{\mathbf{I}}$ is a column vector with unity elements. Maximizing f_1 through differentiation with respect to the elements of $\mathbf{m}$ yields a model parameterized by λ:

$$\mathbf{m}_i = M\frac{e^{-\lambda^t G^{[,i]}}}{Z}, \qquad (4)$$

where the notation $G^{[,i]}$ refers to the ith column of G and the partition function Z preserves the correct normalization. The result so far is typical of Bayesian inverse problems based on an entropy prior and can be applied to a wide variety of problems.

[17] The model formulated above is incomplete, as it does not consider statistical errors in the data. The complete method utilizes the parameterization (4) but also incorporates the error covariance $C_\mathbf{d}$ through the addition of one more constraint:

$$f_2 = S + \lambda^t(\mathbf{d} + e - G\mathbf{m}) + \Lambda\left(e^t C_\mathbf{d}^{-1} e - \Sigma\right). \qquad (5)$$

Here e is a column vector representing experimental errors, Σ is the expectation of χ^2, and Λ is one last Lagrange multiplier imposing a constraint on the error bounds. Both $C_\mathbf{d}$ and χ^2 can be estimated theoretically [*Hysell and Chau*, 2006]. For the purposes of this study, we consider only the diagonal components of $C_\mathbf{d}$ for

simplicity. A constraint need no longer be imposed on the model normalization since that is guaranteed by the parameterization (4).

[18] The spectrum $\mathbf{m}$ is found through extremization of (5). Differentiating with respect to the Lagrange multipliers λ yields the algebraic equation

$$\mathbf{d} + e - G\mathbf{m} = 0, \qquad (6)$$

which is just a restatement of the forward problem. Differentiating with respect to the error terms e yields

$$C_\mathbf{d}\lambda + 2\Lambda e = 0. \qquad (7)$$

Finally, differentiating with respect to Λ yields an equation which relates that term to the others:

$$\Lambda^2 - \frac{\lambda^t C_\mathbf{d} \lambda}{4\Sigma} = 0. \qquad (8)$$

All together, (6), (7), and (8) constitute a system of n coupled algebraic equations for the n components of λ, where n is the number of real-valued data or twice the number of complex autocorrelation function measurements available. Our algorithm amounts to solving the system using a globally convergent solver [*Powell*, 1970]. The algorithm is fast enough to run in real time in this application and exhibits essentially universal convergence.

[19] Figure 3 shows the results of the analysis of the 2 September 2002 data for the group of echoes of interest. The left plots show the normalized autocorrelation function, with real (imaginary) parts plotted in red (blue). We have removed outliers associated with intervals when the receiver was saturated by the transmitter or by clutter, but a few outliers persist. Notice how the lags of the autocorrelation function are clustered in time. This is a consequence of the fact that the radar IPPs were nearly uniform with just a small jitter.

[20] The middle plots of Figure 3 show the spectrum computed using MaxEnt. The spectra are defined, somewhat arbitrarily, at 256 frequencies here. These spectra show broad forms superimposed on flat backgrounds. The background is a combination of clutter and noise. The combination can be estimated and removed easily so long as the signal spectrum is not too broad. Noise can be distinguished from clutter by examining data from clutter-free ranges or transmitter-off intervals. Finally, the right plots of Figure 3 show spectra computed naively by neglecting the jitter in the radar IPP, averaging the ACF estimates sharing nearly the same lag, and using a windowed periodogram (FFT) to produce a 17-point spectrum.

[21] The MaxEnt spectra and the periodograms are rather similar, echoing the findings of *Uppala and*
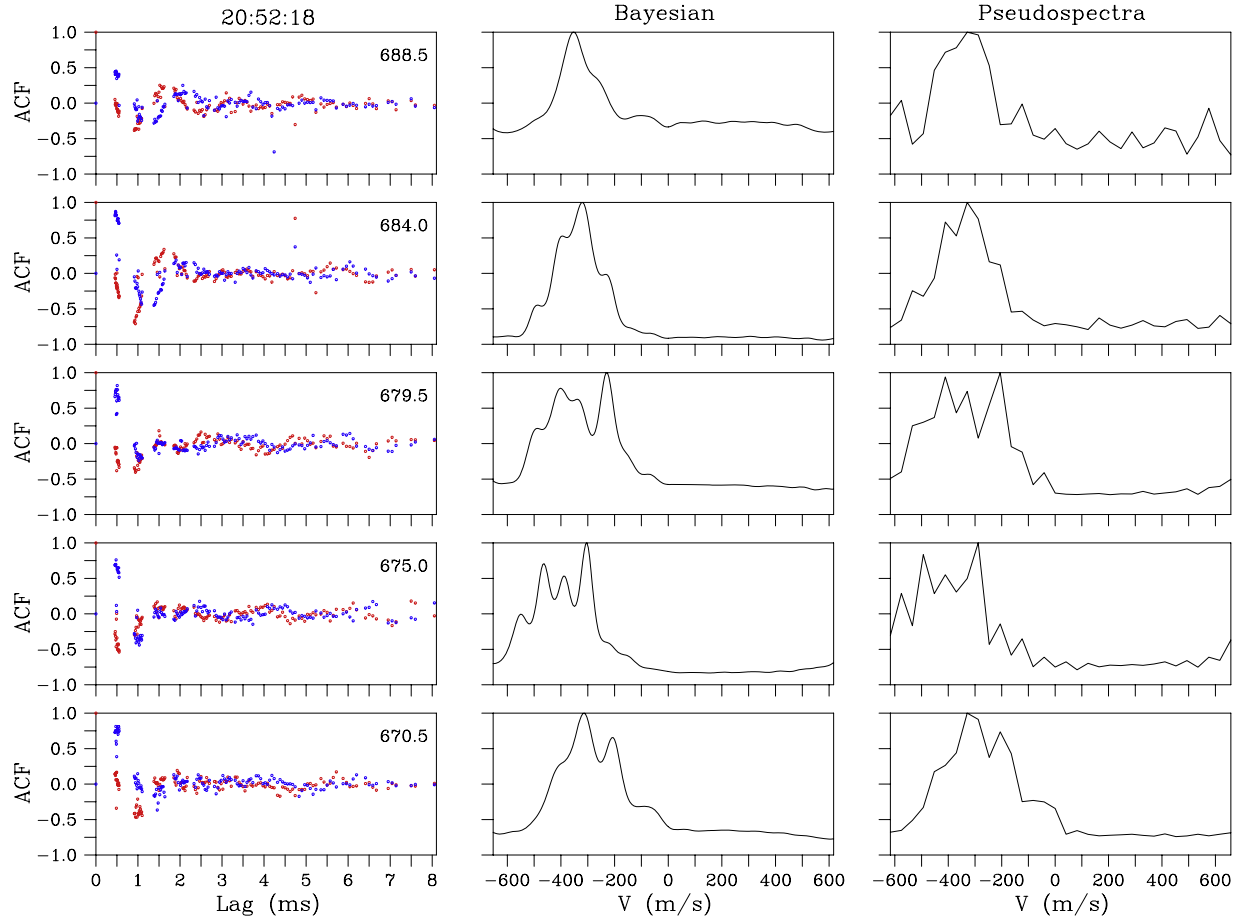
Figure 3. Spectral analysis of the topside echoes from 2 September 2002. (left) Autocorrelation functions versus altitude. Red and blue symbols denote the real and imaginary parts, respectively. (middle) Doppler spectra produced with Bayesian inversion. (right) Doppler spectra produced with periodograms.

Sahr [1994]. Windowing causes the latter to be somewhat broader than the former. The latter also exhibit elevated noise backgrounds, a consequence of the "noise" introduced by misassigning the lag times of the ACFs. Finally, the latter tend to exhibit some spurious ringing. This is a potentially serious problem since it can interfere with the estimation and subtraction of the range clutter introduced by aperiodic pulsing. The MaxEnt spectra are relatively free of ringing, and not by accident. This is a design feature of the inversion algorithm, which suppresses irregularities in the spectra not explicitly supported by the data.

[22] Finally, Figure 4 shows similar results for the 21 February 2006 data. The spectra shown here are qualitatively different from those shown in Figure 3, being dominated mainly by a few narrow spectral lines rather than by a broad continuum. This difference is characteristic of the difference between echoes from inertial regime and collisional regime irregularities [*Hysell*, 2000]. Quantitatively, we can see that the lags of the ACF are distributed more uniformly in time in this experiment than in the previous one. They are still nonuniform, and gaps appear where the receiver was saturated at times. Standard spectral analysis with periodograms is therefore still not rigorous. The same grouping and averaging strategy has nevertheless been applied to produce the curves in Figure 4 (right).

[23] The results are essentially the same as before. The MaxEnt and periodogram spectra are generally similar, but the latter are broader because of windowing and tend to exhibit spurious ringing. The MaxEnt spectra are superimposed on flat backgrounds, facilitating the easy estimation and removal of noise and clutter. There appears to be somewhat more fine structure in the MaxEnt spectra from 2006 than from 2002. All things being equal, we expect improved spectral resolution for
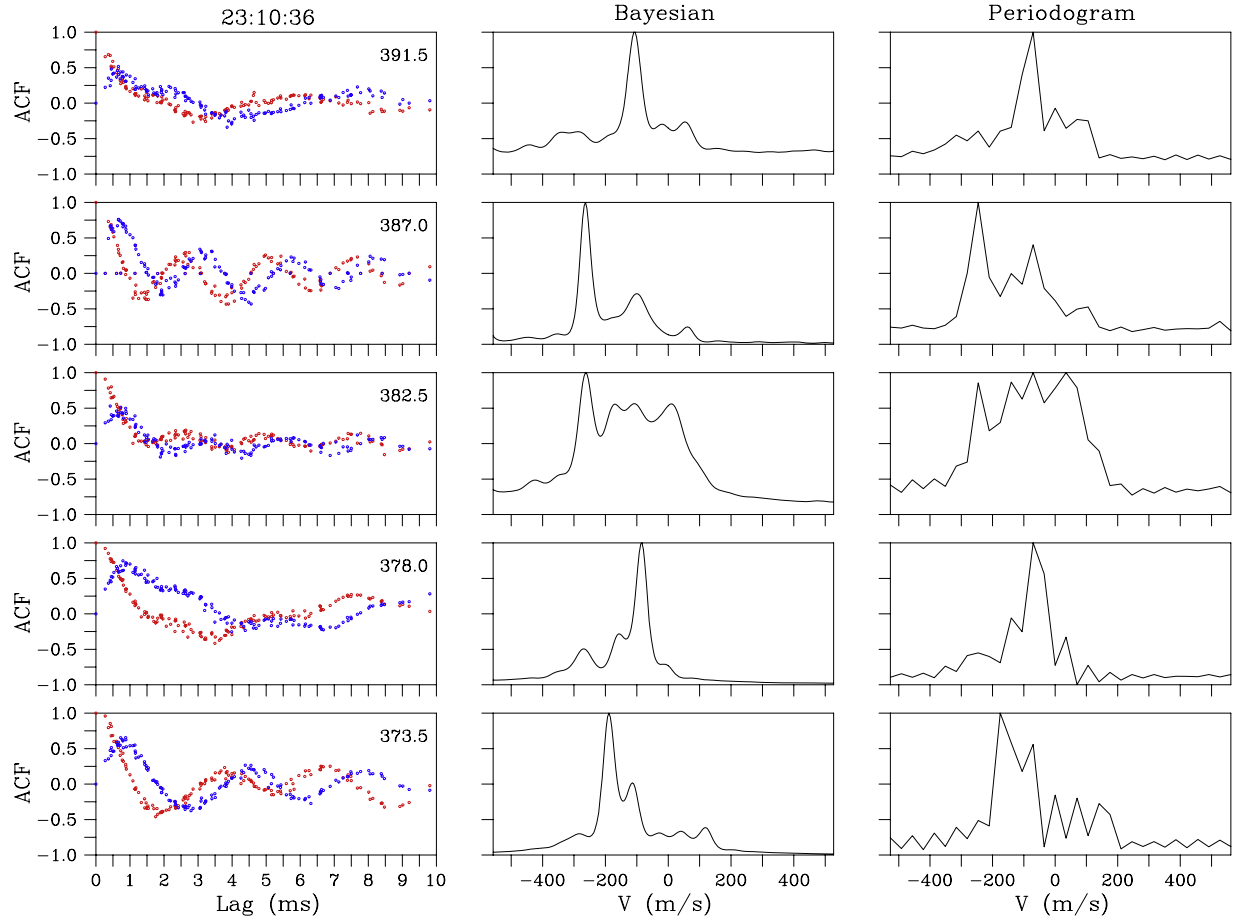
Figure 4. Spectral analysis of the topside echoes from 21 February 2006. (left) Autocorrelation functions versus altitude. Red and blue symbols denote the real and imaginary parts, respectively. (middle) Doppler spectra produced with Bayesian inversion. (right) Doppler spectra produced with periodograms.

the 2006 experiment in view of the greater independence of the corresponding ACF data.

4. Application

[24] This work is a step toward a more ambitious goal of producing aperture synthesis radar images of overspread targets like field-aligned irregularities in ESF plumes over Jicamarca. A prototypical plume image from December 2005 is shown in Figure 5. These data were acquired with spaced receivers using conventional, periodic pulses. Although this particular ESF plume is probably not an example of an inertial regime flow because of its relatively late local time, it exhibits morphological features representative of all plumes, namely, vertical development, spatial intermittency, and fractal-like fine structure. The pixels are color coded, with brightness, hue, and sensitivity representing echo intensity, Doppler shift, and spectral width, respectively (see Figure 5 caption). That most of the image pixels are white or pastel reflects the fact that most of the spectra are flat and that the target is overspread.

[25] Our proximate objective is to measure backscatter with spaced antennas and aperiodic pulses and use them to produce frequency-resolved radar images. Such data can be thought of as being acquired on a grid in space and time, as illustrated in Figure 6. Here spaced antennas and spaced pulses run along the vertical and horizontal axes, respectively. An intersection of an antenna and a pulse represents a sample, and a line connecting two samples represents an element of the data covariance. Each element of the covariance matrix is therefore a function of spatial and temporal lag. The proper placement of the antenna and the pulses assures that no lag is sampled redundantly and that all the lags are sampled quasi-uniformly.
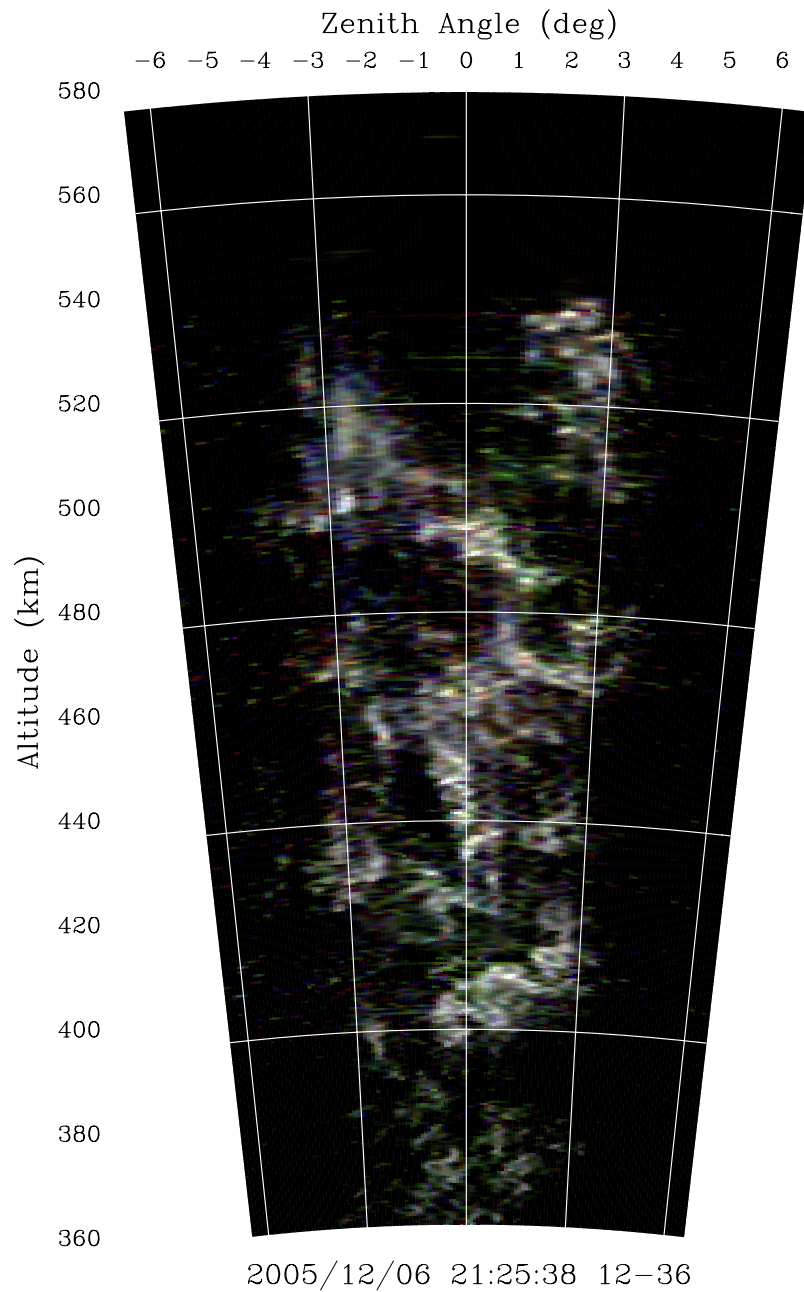
Figure 5. Radar image of a spread F plume over Jicamarca on 6 December 2005. The incoherent integration time for this image was approximately 5 s, and the pixel size is approximately 500 m^2. The brightness of each pixel (total luminosity) is proportional to the signal-to-noise ratio. The hue corresponds to the Doppler frequency, with red (blue) tones reflecting red (blue) Doppler shifts. The saturation corresponds to the spectral width, with saturated (unsaturated) tones indicating narrow (wide) spectra.
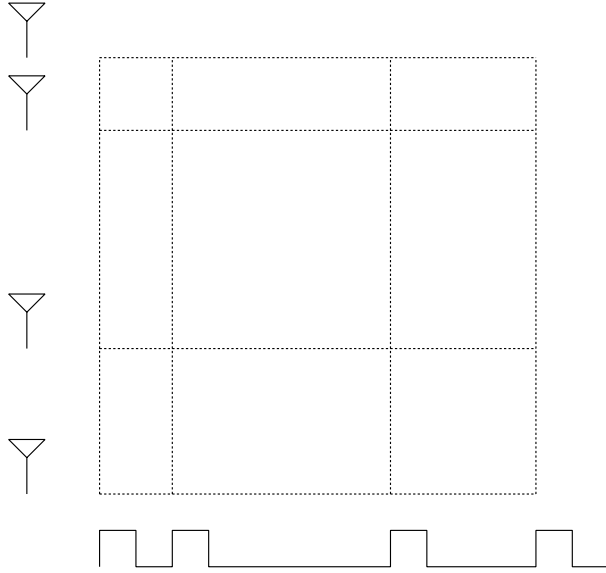
Figure 6. Diagram illustrating aperiodic radar imaging. Data are acquired from different antennas in space and different pulses in a pulse train. The antenna and pulse spacings are chosen to be nonredundant. The cross-correlation function in this space is a function of spatial separation and temporal delay and can be made to be sampled almost uniformly with the appropriate choice of antenna and pulse positions. This cross-correlation function is related to the radar brightness versus bearing and Doppler frequency through a Fourier transform. The transformation can be performed using MaxEnt, as before. In this simplified example, data are acquired at each of the 16 line intersections, so that there would be $(16 \times 15)/2$ distinct cross-spectral baselines to consider for each range gate.

[26] The resulting stationary, homogeneous spatiotemporal visibility function is related to the brightness distribution, the distribution of backscattered power versus bearing ψ and Doppler frequency ω through a single Fourier transform:

$$\langle v(t_i, x_k) v \times (t_j, x_l) \rangle$$
$$= \int \langle |v(\omega, \psi)|^2 \rangle e^{i\omega(t_j - t_i)} e^{ik\psi(x_l - x_k)} d\omega d\psi, \quad (9)$$

where ψ is the direction cosine of the radar wave vector with respect to the direction of the given spaced antenna baseline. The transformation from the visibility data to the brightness model can be accomplished using MaxEnt as it is presently formulated. Frequency aliasing is resolved by the incorporation of a few short IPPs in the pulsing scheme, and range aliasing is resolved by the nonredundant pulse spacings. Analo-

gous statements apply to the spaced antenna placement. Clutter can be removed by subtracting the flat portions of the spectra associated with every image-bearing bin. The only problem is one of scale. Using 8 antennas as is typical at Jicamarca along with 17 pulse positions implies $(136 \times 135)/2 = 9180$ space-time baselines and complex visibilities, necessitating that MaxEnt solves 18,360 simultaneous equations in each range gate. In practice, the technique will almost certainly have to involve fewer pulse positions to be tractable. The flexibility afforded by the "large-excursion" aperiodic pulse scheme will be necessary for sampling the temporal ACF of the echoes uniformly with a modest number of pulses. Uniform sampling has proven beneficial when applying MaxEnt to sparsely sampled visibilities.

[27] Ultimately, we seek to measure a complete Doppler spectrum in every range and arrival angle bin in the radar-illuminated volume. The spectral theory of *Hysell and Chau* [2004] relates the shape of the spectrum to the energy of the irregularities in the scattering volume. According to that theory, which is two dimensional, the ACF of the coherent scatter should be proportional to $\exp[-k_s^2 R(t)]$, where k_s is the scattering wave number and $R(t)$ is the time-integrated diffusivity, defined as $D(t) \equiv \langle x^2 \rangle / 2t$, $x(t)$ being the displacement of a test particle from its initial position in the plane perpendicular to B. The function $R(t)$ can further be shown to be the solution of the equation [*Montgomery*, 1975]

$$\frac{1}{2}\left(\frac{dR}{dt}\right)^2 = \frac{1}{2B^2} \sum_{\mathbf{k}} \left\langle |\mathbf{E}(\mathbf{k})|^2 \right\rangle \left[\frac{1 - \exp(-2k^2 R)}{2k^2}\right], \quad (10)$$

where $\mathbf{k}$ and k are any wave vector and its associated wave number, respectively. The term in angle brackets is the energy spectrum. This may be converted to the power spectrum $\langle |n(\mathbf{k})|^2 \rangle$ using the plasma quasi-neutrality condition. The sum is over wave vectors with wavelengths smaller than the dimension of the scattering volume since longer wavelengths are expected to affect the offset but not the shape of the Doppler spectrum. Concerning the shape of the spectrum, (10) predicts $R(t) \propto t^2$ for short times and $R(t) \propto t$ for long times, implying spectra with shapes that are combination Gaussian and Lorentzian. The actual shape and width of the Doppler spectrum depend both on the underlying energy spectrum and on the size of the scattering volume.

[28] By averaging Doppler spectra over small and large clusters of image pixels, we can determine how the spectrum varies as a function of scattering volume size. Using (10), it should then be possible to invert

this information and estimate the shape of the energy and power spectra of the irregularities. Inversion will be particularly straightforward in the case that the energy spectrum is isotropic, which is predicted for inertial range turbulence. Spectral inferences like this are normally drawn from in situ measurements and are vital for understanding how radio scintillations are produced. The contemporary shortage of instrumented spacecraft flying through the equatorial F region ionosphere motivates the line of investigation outlined here.

5. Summary

[29] We have implemented two strategies for measuring the spectra of moderately overspread radar targets through aperiodic radar pulsing. In the first, the average IPP is made small enough to avoid frequency aliasing, and a slight jitter is introduced in the IPP to resolve ambiguities associated with range aliasing. In the second, the IPP undergoes much more drastic deviation and includes at least a few short lags for wideband spectral estimation. The latter strategy spreads range clutter more widely and produces ACFs with lags more uniformly distributed in time. Clutter bias can be removed so long as the signal spectrum is not too broad. Statistical inverse theory can be used to calculate the spectra of the unevenly sampled data stream in such a way that the noise and clutter background is flat and can be easily estimated and removed.

[30] In our experience, uniform sampling facilitates the inversion of ACFs or visibilities, particularly when the samples are few in number. The two strategies perform comparably here, but we can expect the latter to outperform the former as fewer samples are available for inversion. If the aperiodic pulse technique is merged with the radar-imaging experiment, computational limitations will force a reduction in the number of IPPs and therefore will favor the latter strategy.

[31] A scenario for combining aperiodic pulsing and spaced-receiver radar imaging for observing spread F has also been described. This technique may permit frequency-resolved radar imaging of ESF plumes and other targets and may form the basis of estimates of the irregularity energy and power spectra as functions of wave number. The technique is computationally demanding but conceptually straightforward and should be implemented at Jicamarca in the near future.

References

Chau, J. L., D. L. Hysell, P. M. Reyes, and M. A. Milla (2004), Improved spectral observations of equatorial spread F echoes at Jicamarca using aperiodic transmitter coding, *J. Atmos. Sol. Terr. Phys.*, *66*, 1543.

Farley, D. T. (1969), Incoherent scatter correlation function measurements, *Radio Sci.*, *4*, 935.

Farley, D. T. (1972), Multiple-pulse incoherent-scatter correlation function measurements, *Radio Sci.*, *7*, 661.

Hysell, D. L. (2000), A review and synthesis of plasma irregularities in equatorial spread F, *J. Atmos. Sol. Terr. Phys.*, *62*, 1037.

Hysell, D. L., and J. L. Chau (2004), Interpreting the Doppler spectrum of coherent scatter from topside equatorial spread F, *J. Atmos. Sol. Terr. Phys.*, *66*, 1549.

Hysell, D. L., and J. L. Chau (2006), Optimal aperture synthesis radar imaging, *Radio Sci.*, *41*, RS2003, doi:10.1029/2005RS003383.

Hysell, D. L., and E. B. Shume (2002), Electrostatic plasma turbulence in the topside equatorial F region ionosphere, *J. Geophys. Res.*, *107*(A10), 1269, doi:10.1029/2001JA000227.

Hysell, D. L., M. C. Kelley, W. E. Swartz, and D. T. Farley (1994), VHF radar and rocket observations of equatorial spread F on Kwajalein, *J. Geophys. Res.*, *99*, 15,065.

Jaynes, E. T. (1982), On the rationale of maximum-entropy methods, *Proc. IEEE*, *70*, 939.

Lakshmanan, S. (2006), Extending a Bayesian spectral estimation method for use with unevenly sampled complex radar data, M.S. thesis, Cornell Univ., Ithaca, N. Y.

Lehtinen, M. S., and I. Häggström (1987), A new modulation principle for incoherent scatter measurements, *Radio Sci.*, *22*, 625.

Levanon, N. L. (1988), *Radar Principles*, John Wiley, New York.

Lomb, N. R. (1976), Least squares frequency analysis of unevenly sampled data, *Astrophys. Space Sci.*, *39*, 447.

McDaniel, R. D., and D. L. Hysell (1997), Models and DE II observations of inertial-regime irregularities in equatorial spread F, *J. Geophys. Res.*, *102*, 22,233.

Montgomery, D. (1975), Strongly magnetized classical plasma models, in *Plasma Physics*, edited by C. DeWitt and J. Peyraud, p. 425, Gordon and Breach, New York.

Powell, M. J. D. (1970), A hybrid method for nonlinear equations, in *Numerical Methods for Nonlinear Algebraic Equations*, edited by P. Rabinowitz, p. 87, Gordon and Breach, London.

Press, W. H., B. P. Flannery, S. A. Teukolsky, and W. T. Vetterling (1988), *Numerical Recipes in C*, Cambridge Univ. Press, New York.

Qi, Y., T. P. Minka, and R. W. Picard (2002), Bayesian spectrum estimation of unevenly sampled nonstationary data, *Tech. Rep. Vismod-TR-556*, Mass. Inst. of Technol. Media Lab., Cambridge, Mass.

Sahr, J. D., D. T. Farley, and W. E. Swartz (1989), Removal of aliasing in pulse-to-pulse Doppler radar measurements, *Radio Sci.*, *24*, 697.

Scargle, J. D. (1982), Statistical aspects of spectral analysis of unevenly sampled data, *Astrophys. J.*, *263*, 835.

Shume, E. B., and D. L. Hysell (2004), Spectral analysis of plasma drift measurements from the AE-E satellite: Evidence of an inertial subrange in equatorial spread *F*, *J. Atmos. Sol. Terr. Phys.*, *66*, 57.

Skilling, J., and R. K. Bryan (1984), Maximum entropy image reconstruction: General algorithm, *Mon. Not. R. Astron. Soc.*, *211*, 111.

Sulzer, M. P. (1986), A radar technique for high range resolution incoherent scatter autocorrelation function measurements utilizing the full average power of klystron radars, *Radio Sci.*, *21*, 1033.

Uppala, S. V. (1993), Aperiodic radar technique for the spectrum estimation of moderately overspread targets, M.S. thesis, Univ. of Wash., Seattle.

Uppala, S. V., and J. D. Sahr (1994), Spectrum estimation of moderately overspread radar targets using aperiodic transmitter coding, *Radio Sci.*, *29*, 611.

Wingham, D. J. (1992), The reconstruction of a band-limited function and its Fourier transform from a finite number of samples at arbitrary locations by singular value decomposition, *IEEE Trans. Signal Process.*, *40*, 559.

Zargham, S., and C. E. Seyler (1989), Collisional and inertial dynamics of the ionospheric interchange instability, *J. Geophys. Res.*, *94*, 9009.

J. L. Chau, Radio Observatorio de Jicamarca, Instituto Geofísico del Perú, Apartado 13-0207, Lima 13, Perú.

D. L. Hysell, Department of Earth and Atmospheric Sciences, Cornell University, Ithaca, NY 14853, USA. (dlh37@cornell.edu)

S. Lakshmanan, Raytheon Company, 225 Presidential Way, Woburn, MA 01801, USA.